



Engineering Notes

Guidance Solutions for Spacecraft Planar Rephasing and Rendezvous Using Input Shaping

Margaret Lawn,* Giuseppe Di Mauro,[†] and
Riccardo Bevilacqua[‡]
University of Florida, Gainesville, Florida 32611

DOI: 10.2514/1.G002910

I. Introduction

THE use of small satellites flying in close proximity is increasing at a rapid pace for many types of missions, including space science, Earth observation and remote sensing, Earth science, and technology demonstration [1]. Thanks in part to the growth in popularity of the CubeSat standard and related components and technologies, small satellites (herein defined as those satellites with a wet mass less than 500 kg) are generally more economical to design and launch than large satellites [2,3]. Several small satellites flying in formation can perform the tasks assigned to a single large satellite while providing increased adaptability, versatility, and robustness. A small satellite formation can be reconfigured as mission directives change or to take on a pattern better suited to its task. It may be adjusted to compensate for a single malfunctioning vehicle without necessitating a mission abort. The formation could even be separated and viable individual satellites reassigned to other missions at the end of the original mission lifetime.

However, small satellites present their own variety of design challenges, especially in the areas of guidance, navigation, and control (GNC). The primary obstacle is limited onboard storage space, which restricts both available power and propulsion system complexity. High-performance space-qualified onboard computers require high power to work; thus, small spacecraft generally have limited computing capability. Moreover, in order to meet the physical dimension constraints, they are typically equipped with small thrusters providing low thrust and operating only in on/off configurations with a few set force magnitudes. In addition, most satellite configurations require a level of onboard autonomy to guarantee highly accurate performance and an efficient and prompt response to contingencies. This implies that GNC solutions must be computed on board to meet mission requirements.

In light of the aforementioned information, efficient relative orbit control techniques must be developed to satisfy the low-thrust

constraints without reducing performance accuracy or straining the limited computational power of the small onboard systems. Many approaches have been investigated for relative motion control, including impulsive and continuous strategies. Chernick and D'Amico developed an impulsive strategy for relative motion control that included the effects of J_2 [4]. In further details, they computed the semianalytical solution for in-plane relative motion control by inverting the linearized equations of relative motion parameterized using the mean relative orbit elements. Shaub et al. developed a continuous nonlinear feedback control law based on the Lyapunov theory to reestablish a desired J_2 invariant relative orbit by formalizing the relative motion in terms of mean orbit element differences [5].

In this Note, the input-shaping approach is investigated to derive the guidance solution for spacecraft planar rephasing and rendezvous maneuver. Input shaping is a technique consisting of the convolution of a feedforward control signal with a series of delayed impulses. The temporal distribution and magnitudes of these impulses depend on the natural frequency and damping of the system, respectively [6]. This technique has been extensively examined for vibration suppression of flexible manipulators; more recently, it has been proposed for orbital maneuvering of spacecraft systems [7]. It is worth pointing out that input shaping is not intended to reduce the energy of the system, i.e., it cannot damp the system oscillations completely. However, an appropriate choice of the shaper's parameters enables the modification of the system's oscillatory behavior. In the context of spacecraft relative maneuvering, this means that input shaping can be exploited to maneuver the satellite from one equilibrium configuration to another, where equilibrium means a nondrifting relative state, modifying the periodic relative motion [8]. In this Note, the input-shaping method is proposed to compute the guidance solutions to the problems of short-distance planar spacecraft rephasing and rendezvous when continuous low thrust is used. The angle of the in-plane thrust vector is assumed to be a fixed user-specified parameter, which is a freedom not considered in previous research, wherein thrust was confined to the alongtrack direction only.

The main contribution of this Note consists of deriving an analytical guidance solution, including the effects of J_2 perturbation, for planar spacecraft rephasing and rendezvous maneuvers, which could be easily implemented on board small spacecraft with a low-thrust propulsion system and limited computing capabilities. The second important contribution is the demonstrated ability to easily and quickly compute minimum-fuel maneuvers using such analytical solutions.

The rest of the Note is organized as follows. In the first section, the spacecraft relative dynamics model and its analytical solution are presented. In the next section, two types of shapers, the zero vibration shaper and the zero vibration derivative shaper, are introduced and the shaper profiles are described. The subsequent section is dedicated to the derivation of analytical solutions for the final state, the center of final relative ellipse, the final relative eccentricity, and the condition for final orbit equilibrium. Then, the guidance trajectories obtained using the shaped thrust profile and spacecraft dynamics model are presented. The final section shows optimization of the shaper parameters to obtain a desired relative eccentricity while minimizing control action.

II. Dynamics Model

Unlike the work presented by one of the authors of this Note in [7], this study uses a more accurate relative dynamics model to derive the analytical guidance law through the input-shaping technique. This model, developed by Schweighart and Sedwick (SS), includes the

Presented at the 27th AAS/AIAA Space Flight Mechanics Meeting, San Antonio, TX, 6–9 February 2017; received 17 March 2017; revision received 12 June 2017; accepted for publication 14 June 2017; published online Open Access 24 July 2017. Copyright © 2017 by Riccardo Bevilacqua. Published by the American Institute of Aeronautics and Astronautics, Inc., with permission. All requests for copying and permission to reprint should be submitted to CCC at www.copyright.com; employ the ISSN 0731-5090 (print) or 1533-3884 (online) to initiate your request. See also AIAA Rights and Permissions www.aiaa.org/randp.

*Graduate Student, Department of Mechanical and Aerospace Engineering, ADAMUS Laboratory, 939 Sweetwater Dr.

[†]Postdoctoral Associate, Department of Mechanical and Aerospace Engineering, ADAMUS Laboratory, 939 Sweetwater Dr.

[‡]Associate Professor, Department of Mechanical and Aerospace Engineering, ADAMUS Laboratory, 939 Sweetwater Dr. Senior Member AIAA.

effects of the second-order perturbative term of the Earth's geopotential by adding the linearized J_2 force as a forcing function [9]. This leads to the following set of linearized constant-coefficient differential equations of relative motion [10]:

$$\begin{aligned} \ddot{x} - 2\bar{m}\dot{y} - (4\bar{m}^2 - \bar{n}^2)x &= u_x \\ \ddot{y} + 2\bar{n}\dot{x} &= u_y \end{aligned} \quad (1)$$

$$\ddot{z} + (2\bar{m}^2 - \bar{n}^2)z = u_z \quad (2)$$

where

$$\begin{aligned} k_{j_2} &= \frac{3}{8} J_2 \frac{R_e^2}{r_{\text{ref}}^2} \left(1 + 3 \cos(2i_{\text{ref}}) \right), & \bar{m} &= n_{\text{ref}} \sqrt{1 + k_{j_2}}, \\ \bar{n} &= n_{\text{ref}} \sqrt{1 - k_{j_2}} \end{aligned} \quad (3)$$

with $J_2 = 0.0010827$, and R_e as the mean Earth radius. The preceding equations are expressed in the local vertical, local horizontal (LVLH) reference frame initially centered in the chief's center of mass and moving on a circular orbit of radius r_{ref} and inclination i_{ref} with the rotational rate n_{ref} . Note that x points radially away from the planet to the reference satellite, z is the direction of the orbit's angular momentum, and y completes the right-handed orthonormal basis. Although accurately describing the relative motion under the effect of J_2 potential, the SS equations can still be solved analytically and then ease the derivation of the analytical guidance solution.

From Eqs. (1) and (2), it is clear that the motion in the z direction is decoupled from the motion in the x and y directions. For this reason, we consider only the in-plane (x - y) dynamics in this study. The analytical solution to the SS equations for planar motion is the following:

$$\begin{aligned} \begin{Bmatrix} x_f \\ y_f \\ \dot{x}_f \\ \dot{y}_f \end{Bmatrix} &= \Phi(t, t_0) \begin{Bmatrix} x_0 \\ y_0 \\ \dot{x}_0 \\ \dot{y}_0 \end{Bmatrix} + \Psi(t) \begin{Bmatrix} u_x \\ u_y \end{Bmatrix} \\ \Phi(t, t_0) &= \begin{bmatrix} \frac{a^2}{\bar{n}^2} - \frac{b}{\bar{n}^2} \cos(\bar{n}t) & 0 & \frac{\sin(\bar{n}t)}{\bar{n}} & \frac{a}{\bar{n}^2} (1 - \cos(\bar{n}t)) \\ -\frac{ab}{\bar{n}^2} \left(dt - \frac{\sin(\bar{n}t)}{\bar{n}} \right) & 1 - \frac{a}{\bar{n}^2} (1 - \cos(\bar{n}t)) & \frac{a^2}{\bar{n}^2} \sin(\bar{n}t) - \frac{b}{\bar{n}^2} dt & \\ b \left(\frac{\sin(\bar{n}t)}{\bar{n}} \right) & 0 & \cos(\bar{n}t) & \frac{a}{\bar{n}} \sin(\bar{n}t) \\ -\frac{ab}{\bar{n}^2} (1 - \cos(\bar{n}t)) & 0 & -\frac{a}{\bar{n}} \sin(\bar{n}t) & \frac{a^2}{\bar{n}^2} \cos(\bar{n}t) - \frac{b}{\bar{n}^2} \end{bmatrix} \\ \Psi(t, t_0) &= \begin{bmatrix} \frac{1}{\bar{n}^2} (1 - \cos(\bar{n}t)) & \frac{a}{\bar{n}^2} \left(dt - \frac{\sin(\bar{n}t)}{\bar{n}} \right) \\ -\frac{a}{\bar{n}^2} \left(dt - \frac{\sin(\bar{n}t)}{\bar{n}} \right) & \frac{(\bar{n}^2 + b)}{\bar{n}^4} (1 - \cos(\bar{n}t)) - \frac{b}{\bar{n}^2} \frac{dt^2}{2} \\ \frac{\sin(\bar{n}t)}{\bar{n}} & \frac{a}{\bar{n}^2} (1 - \cos(\bar{n}t)) \\ -\frac{a}{\bar{n}^2} (1 - \cos(\bar{n}t)) & \frac{\sin(\bar{n}t)}{\bar{n}} + \frac{b}{\bar{n}^2} \left(\frac{\sin(\bar{n}t)}{\bar{n}} - dt \right) \end{bmatrix} \end{aligned} \quad (4)$$

where

$$a = 2\bar{m} \quad b = 5\bar{m}^2 - 2n_{\text{ref}}^2 \quad dt = t - t_0 \quad (5)$$

III. Input-Shaper Basics

The main idea of the input-shaping method is based on the convolution of the command signal with a sequence of Dirac impulses. These impulses must be applied in specified moments of

time and with specified amplitude in order to nullify the residual vibrations of the system [6].

This study investigates two classes of shapers, namely, the zero vibration (ZV) shaper and the zero vibration derivative (ZVD) shaper. They are used to shape a bang–bang thrust profile of amplitude \bar{u} .

A. Zero Vibration Shaper

The ZV shaper is probably the simplest input shaper. It is designed to filter an incoming signal such that the system driven by the new shaped command will not have vibration arising from the frequency filtered out by the ZV shaper [11]. It consists of two impulses for which the temporal distribution and magnitudes are

$$T = [t_1, t_2] = [0 \quad \Delta t] \quad (6)$$

$$A = [A_1, A_2] = \left[\frac{\zeta}{\zeta + 1}, \frac{1}{\zeta + 1} \right] \quad (7)$$

where

$$\zeta = e^{\zeta\pi} / \sqrt{1 - \zeta^2} \quad (8)$$

with ζ the damping ratio of the system. The values T and A are the time by which each impulse is delayed and its corresponding amplitude. Note that, when $\Delta t = \pi/\omega_d$, where ω_d indicates the damped natural frequency of the system, the command shaper described by Eqs. (6–8) will suppress the system residual vibrations.

For the purpose of deriving a control profile for the in-plane deputy maneuvering, the aforementioned shaper can be used to shape a bang–bang continuous command of amplitude \bar{u} . In further detail, let us assume that the deputy provides a continuous thrust

$$U = [u_x, u_y]^T = [u \sin(\alpha), u \cos(\alpha)]^T$$

where u is the shaped bang–bang command, and α is a fixed user-specified parameter defined as the angle between the in-plane projection of control vector and the y axis of the LVLH reference frame. Then, the shaped control command can be formulated as follows:

$$u = A_1 f_{t1} + A_2 f_{t2} \quad (9)$$

where

$$\begin{aligned} f_{t1} &= \begin{cases} 0 & t > t^* \\ \bar{u} \text{sign}(\bar{y}_d - y_0) & t < t^*/2 \\ -\bar{u} \text{sign}(\bar{y}_d - y_0) & t^*/2 < t < t^* \end{cases} \\ f_{t2} &= f_{t1}(t - \Delta t) \end{aligned} \quad (10)$$

where y_0 is the initial relative alongtrack position, \bar{y}_d is the desired alongtrack position of the center of the ellipse representing the final relative motion, and t^* is the bang–bang time (i.e., $t^*/2$ is the bang–bang switching time). Note that the impulse delay Δt has to be lower than $t^*/2$. Moreover, the impulse magnitudes A_i are equal to 0.5 because the damping of the in-plane dynamics described by Eq. (1) is $\zeta = 0$.

B. Zero Vibration Derivative Shaper

The formulation of the ZVD shaper is similar to that of the ZV shaper. However, the ZVD shaper provides higher robustness to modeling errors by forcing the derivative of the vibration amplitude with respect to the frequency to be zero [12]. The cost of the added robustness is a longer time to cancel the residual oscillation of the system. The ZVD consists of three impulses for which the temporal distribution and magnitudes are

$$T = [t_1, t_2, t_3] = [0 \quad \Delta t \quad 2\Delta t] \quad (11)$$

$$A = [A_1, A_2, A_3] = \left[\frac{\zeta^2}{\zeta^2 + 2\zeta + 1}, \frac{2\zeta}{\zeta^2 + 2\zeta + 1}, \frac{1}{\zeta^2 + 2\zeta + 1} \right] \quad (12)$$

with ζ given by Eq. (8). In accordance with the analysis carried out in the previous section, the ZVD shaped input vector

$$U = [u_x, u_y]^T = [u \sin(\alpha), u \cos(\alpha)]^T$$

can be formulated as follows:

$$u = A_1 f_{t1} + A_2 f_{t2} + A_3 f_{t3} \quad (13)$$

where

$$f_{t1} = \begin{cases} 0 & t > t^* \\ \bar{u} \operatorname{sign}(\bar{y}_d - y_0) & t < t^*/2 \\ -\bar{u} \operatorname{sign}(\bar{y}_d - y_0) & t^*/2 < t < t^* \end{cases}$$

$$f_{t2} = f_{t1}(t - \Delta t)$$

$$f_{t3} = f_{t1}(t - 2\Delta t) \quad (14)$$

Here, the impulse delay Δt is constrained to be lower than $t^*/4$, and the impulses' magnitudes are $A_{1,3} = 1/4$ and $A_2 = 1/2$.

For the sake of example, Fig. 1 shows the thrust profile shaped through the ZVD and ZV shapers, respectively, when $\bar{y}_d < y_0$.

$$A = \sqrt{(4\bar{m}^2 - \bar{n}^2)} \begin{pmatrix} 16\bar{m}^4 x_0^2 + 4\bar{m}^2 \dot{y}_0^2 - \bar{n}^2 \dot{y}_0^2 - \bar{n}^2 \bar{u}_y y_0 + \bar{n}^2 \bar{u}_y \bar{y}_d \\ + 16\bar{m}^3 x_0 \dot{y}_0 + 2\bar{m} \bar{u}_y \dot{x}_0 - 4\bar{m}^2 \bar{n}^2 x_0^2 + 8\Delta t \bar{m}^3 \bar{u}_y x_0 \\ + 4\Delta t \bar{m}^2 \bar{u}_y \dot{y}_0 - \Delta t \bar{n}^2 \bar{u}_y \dot{y}_0 - 4\bar{m} \bar{n}^2 x_0 \dot{y}_0 - 2\Delta t \bar{m} \bar{n}^2 \bar{u}_y x_0 \end{pmatrix} \quad (18)$$

IV. Input-Shaping Analytical Guidance

This section presents the steps to derive the closed-form solutions for the final relative state and eccentricity when the ZV and ZVD shapers are implemented. The process is as follows. First, the expressions for the in-plane final state X_f and alongtrack location of the center of the final ellipse \bar{y} are computed. Given a desired alongtrack location of the center of the final ellipse \bar{y}_d , the expression for \bar{y} is solved for the necessary bang-bang time t^* , which results in $\bar{y} = \bar{y}_d$ at the end of the maneuver. Then, the requirements for an equilibrium final condition are determined. Finally, an expression for the final relative eccentricity is derived as a function of X_0 , t^* , Δt , \bar{m} , \bar{n} , \bar{u} , and α .

A. ZV Shaper

Using the analytical SS solution given by Eq. (4) with the filtered control signal given by Eq. (9) and the generic initial condition $X_0 = [x_0 \ y_0 \ \dot{x}_0 \ \dot{y}_0]$, the in-plane final state can be computed as given by Eq. (A1) listed in Appendix A. The alongtrack location of the center of the ellipse representing the final relative orbit is given by the following formula [13]:

$$\bar{y} = y_f - \frac{2\dot{x}_f \bar{m}}{\bar{n}^2} \quad (15)$$

Using the expression of the final state reported in Eq. (A1), Eq. (15) can be rearranged as follows:

$$\bar{y} = f(X_0, t^*, \Delta t, \bar{m}, \bar{n}, \alpha, \bar{u})$$

$$= \frac{-1}{4\bar{n}^2} [8\bar{m}\dot{x}_0 - 4\bar{n}^2 y_0 + 32\bar{m}^3 t^* x_0 + 16\bar{m}^2 t^* \dot{y}_0 - 4\bar{n}^2 t^* \dot{y}_0 - 4\bar{m}^2 t^{*2} \bar{u}_y + \bar{n}^2 t^{*2} \bar{u}_y + 32\Delta t \bar{m}^3 \dot{y}_0 + 16\Delta t \bar{m}^2 \dot{y}_0 - 4\Delta t \bar{n}^2 \dot{y}_0 - 8\Delta t \bar{m} \bar{n}^2 x_0 - 8\bar{m} \bar{n}^2 t^* x_0] \quad (16)$$

where $\bar{u}_y = \bar{u} \cos(\alpha)$ and $\bar{u}_x = \bar{u} \sin(\alpha)$. Then, Eq. (16) can be solved for the bang-bang time t^* such that $\bar{y}(t^*) = \bar{y}_d$, i.e.,

$$t^* = \frac{2}{\bar{u}_y (4\bar{m}^2 - \bar{n}^2)} [8\bar{m}^3 x_0 + 4\bar{m}^2 \dot{y}_0 - 2\bar{m} \bar{n}^2 x_0 - \bar{n}^2 \dot{y}_0 \pm A] \quad (17)$$

where

To obtain a closed, nondrifting relative orbit at the end of maneuver, the following conditions must be satisfied [14]:

$$\dot{y}_f = -2\bar{m}x_f \quad (19)$$

or, equivalently

$$\bar{x} = 4x_f + \frac{2\dot{y}_f}{\bar{m}} = 0 \quad (20)$$

where \bar{x} represents the radial location of the center of the final ellipse. Using the final state equations obtained through the application of the

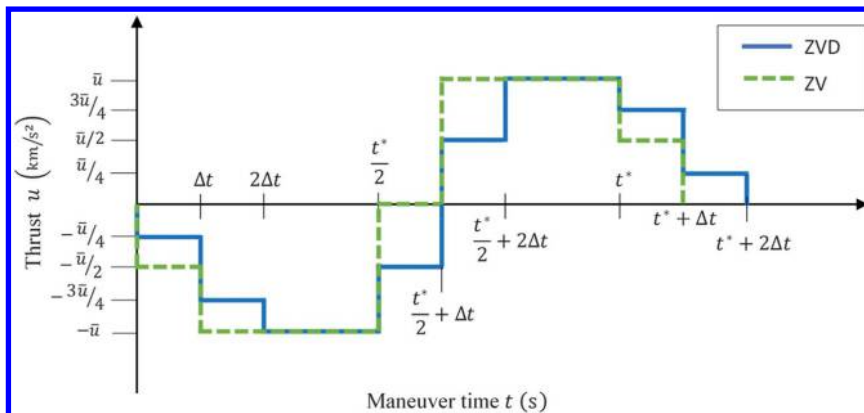


Fig. 1 Shaped control profile.

shaped control profile [i.e., Eq. (A1)], the term \bar{x} becomes

$$\bar{x} = 4x_f + \frac{2\dot{y}_f}{\bar{m}} = 4x_0 + \frac{2\dot{y}_0}{\bar{m}} \quad (21)$$

This indicates that the application of the thrust profile described by Eqs. (9) and (10) guarantees a nondrifting closed relative orbit if the initial motion is an equilibrium. If the initial motion is not an equilibrium, the final motion may drift from the desired final orbit after the conclusion of the maneuver. The eccentricity of the final relative orbit is given by the following formula [13]:

$$e_{\text{rel},f} = \sqrt{(x_f - \bar{x})^2 + ((y_f - \bar{y})/2)^2} \quad (22)$$

The relative eccentricity can be written as a function of X_0 , t^* , Δt , \bar{m} , \bar{n} , \bar{u} , and α , substituting the expression of the final state [Appendix A, Eq. (A1)] in Eq. (22). The final form is listed as Eq. (C1) (see Appendix C).

B. ZVD Shaper

Substituting the ZVD control signal given by Eq. (13) in Eq. (4), considering a set of generic initial conditions $X_0 = [x_0 \ y_0 \ \dot{x}_0 \ \dot{y}_0]$, leads to the final state reported in Eq. (B1) (see Appendix B). As discussed in the previous section for the ZV shaper, the alongtrack location of the center of the final relative ellipse is given by the following formula:

$$\begin{aligned} \bar{y} = y_f - \frac{2\dot{x}_f\bar{m}}{\bar{n}^2} = \frac{-1}{4\bar{n}^2} & \left[8\bar{m}\dot{x}_0 - 4\bar{n}^2y_0 + 32\bar{m}^3t^*x_0 + 16\bar{m}^2t^*\dot{y}_0 \right. \\ & - 4\bar{n}^2t^*\dot{y}_0 - 4\bar{m}^2t^{*2}\bar{u}_y + \bar{n}^2t^{*2}\bar{u}_y + 64\Delta t\bar{m}^3x_0 + 32\Delta t\bar{m}^2\dot{y}_0 \\ & \left. - 8\Delta t\bar{n}^2\dot{y}_0 - 16\Delta t\bar{m}\bar{n}^2x_0 - 8\bar{m}\bar{n}^2t^*x_0 \right] \end{aligned} \quad (23)$$

The bang–bang time t^* can be computed by solving $\bar{y}(t^*) = \bar{y}_d$, which yields

$$t^* = \frac{2}{\bar{u}_y(4\bar{m}^2 - \bar{n}^2)} \left[8\bar{m}^3x_0 + 4\bar{m}^2\dot{y}_0 - 2\bar{m}\bar{n}^2x_0 - \bar{n}^2\dot{y}_0 \pm A \right] \quad (24)$$

where

$$A = \sqrt{(4\bar{m}^2 - \bar{n}^2) \left(\begin{aligned} & 16\bar{m}^4x_0^2 + 4\bar{m}^2\dot{y}_0^2 - \bar{n}^2\dot{y}_0^2 - \bar{n}^2\bar{u}_y y_0 + \bar{n}^2\bar{u}_y \bar{y}_d \\ & + 16\bar{m}^3x_0\dot{y}_0 + 2\bar{m}\bar{u}_y\dot{x}_0 - 4\bar{m}^2\bar{n}^2x_0^2 + 16\Delta t\bar{m}^3\bar{u}_y x_0 \\ & + 8\Delta t\bar{m}^2\bar{u}_y\dot{y}_0 - 2\Delta t\bar{n}^2\bar{u}_y\dot{y}_0 - 4\bar{m}\bar{n}^2x_0\dot{y}_0 - 4\Delta t\bar{m}\bar{n}^2\bar{u}_y x_0 \end{aligned} \right)} \quad (25)$$

Also, for the ZVD case, the nondrifting condition $\bar{x} = 0$ (i.e., $\dot{y}_f = -2\bar{m}x_f$) at the end of the maneuver, $t_m = t^* + 2\Delta t$ is satisfied if the initial motion is an equilibrium. In other words, Eq. (21) is still valid.

Ultimately, the eccentricity of the final relative orbit can be computed through Eqs. (22) and (B1), and it is listed in Appendix D as Eq. (D1).

V. Numerical Simulations

This section presents the guidance trajectories obtained using the thrust profile derived in the previous sections and the initial relative states listed in Table 1. Two different scenarios are considered hereafter. For the first one (case 1), the initial relative state is a leader–follower initial condition for the linear equations [Eq. (1)], i.e., no x displacement or relative velocity. For the second scenario (case 2), the initial condition is an equilibrium motion, i.e., $\dot{y}_0 = -2\bar{m}x_0$. Table 1 summarizes the initial relative state X_0 for both scenarios.

Table 1 Initial state X_0 for studied cases

Simulation scenarios	x_0 , km	y_0 , km	\dot{x}_0 , km/s	\dot{y}_0 , km/s
Case 1	0	-4.258	0	0
Case 2	-0.604	-4.258	0.0004	0.0014

Table 2 Parameters for studied cases

Parameter	Value
\bar{m} , 1/s	$1.1309e - 3$
\bar{n} , 1/s	$1.1317e - 3$
T , s	$5.5517e + 03$
r_{ref} , km	6778.1363
n_{ref} , 1/s	$1.1313e - 3$
k_{J_2}	$-6.7728e - 04$

Table 2 lists additional parameters used in the following simulations. It should also be noted that the reference orbit is circular with an inclination of 97.99 deg.

The initial relative eccentricities

$$e_{\text{rel},0} = \sqrt{\left[x_0 - \left(4x_0 + \frac{2\dot{y}_0}{\bar{m}} \right) \right]^2 + \left[\frac{y_0 - (y_0 + (2\dot{x}_0\bar{m}/\bar{n}^2))}{2} \right]^2} \quad (26)$$

for cases 1 and 2 are 0 and 0.6792, respectively. For all sample cases, the maximum thrust magnitude is assumed to be $\bar{u} = 2 \cdot 10^{-8}$ km/s² and the desired alongtrack location of the center of the final relative ellipse is $\bar{y}_d = 0$.

As a first example, for case 1 with $\alpha = 45$ deg and $\Delta t/T = 0.5$, with $T = 2\pi/\bar{n}$, the relative state components evolve over the course of the maneuver times: $t_m = t^* + \Delta t$ and $t_m = t^* + 2\Delta t$ for ZV and ZVD, respectively, according to Fig. 2. It can be verified by this example that using the ZVD shaper results in a longer time than the ZV shaper to nullify the oscillations introduced to the system by the control accelerations. In Fig. 3, the equations of the final relative eccentricities [Eqs. (C1) and (D1)] are plotted over a range of $\Delta t/T$ values: for case 1 (left) and case 2 (right) when $\alpha = 45$ deg. For case 1, the minimum final relative eccentricity $e_{\text{rel},f}$ is zero when

$\Delta t/T = 0.5$ for both ZV and ZVD shapers. The maximum $e_{\text{rel},f}$ is obtained when $\Delta t/T = 0$ or $\Delta t/T = 1$ for both classes of shapers. Note that the value of Δt must be lower than $t^*/2$ and $t^*/4$ for ZV and ZVD solutions, respectively. In light of this, because the bang–bang times t^* are 5.57 and 5.962 h for case 1 and case 2, respectively, the value of $\Delta t/T$ must be 0.9 at most when the ZVD shaper is implemented, for both simulated cases. For case 2 using the ZV shaper, $\Delta t/T = 0.3134$ yields the minimum $e_{\text{rel},f}$ and $\Delta t/T = 0.8209$ yields the maximum $e_{\text{rel},f}$. Additionally, when the ZVD shaper is used, $\Delta t/T = 0.1891$ yields the minimum $e_{\text{rel},f}$ and $\Delta t/T = 0.8519$ yields the maximum $e_{\text{rel},f}$. For case 2, it is clear that neither shaper can completely damp the system oscillation (i.e., force $e_{\text{rel},f}$ to zero). In fact, the shapers are designed to suppress the vibrations introduced by maneuver control input rather than to cancel the existing initial oscillations. However, for both cases and both shapers, the final relative eccentricity matches the initial relative eccentricity when $\Delta t/T = 0.5$. Figure 3 also visualizes the higher

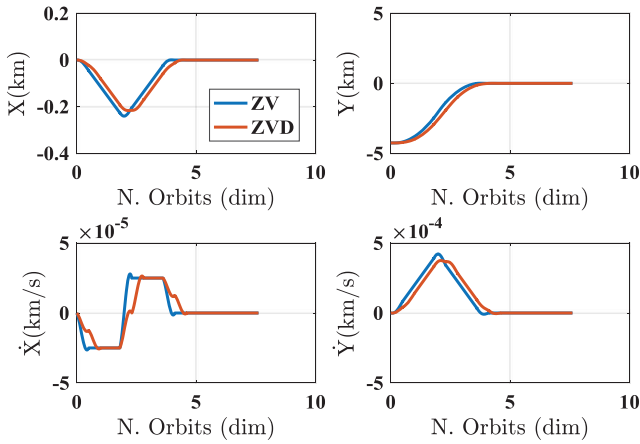


Fig. 2 Relative state vector components resulting from ZV and ZVD shaping for case 1 (N, number; dim, dimensionless).

robustness to the system uncertainties of the ZVD shaper with respect to the ZV shaper. For the sake of simplicity, let us consider the case 1 reported in Fig. 3a. It is clear that, in the vicinity of the zero eccentricity condition, an error on the system frequency (i.e., on the design parameter Δt) causes a rapid increase of the final eccentricity when the ZV shaper is used. On the contrary, the ZVD shaper produces a smaller variation of the final eccentricity in presence of an

error on the system frequency because it sets the derivative of the vibration amplitude with respect to the frequency equal to zero [11]. In the following figures, guidance trajectories are plotted for each case and each shaper using the values of $\Delta t/T$ calculated previously when $\alpha = 45$ deg. The three plots in each figure use $\Delta t/T$ values that result in minimum, intermediate, and maximum final relative eccentricities.

Figures 4 and 5 show trajectories using case 1 initial conditions when the ZV and ZVD are applied, respectively. The values of $\Delta t/T$ used are 0 (for maximum $e_{rel,f}$), 0.25 (for intermediate $e_{rel,f}$), and 0.5 (for minimum $e_{rel,f}$).

Figures 6 and 7 show the control input components corresponding to the trajectories shown in Figs. 4 and 5 when the ZV and ZVD shapers are applied, respectively.

Figures 8 and 9 illustrate the guidance trajectories using case 2 initial conditions when the ZV and ZVD shapers are applied, respectively. The values of $\Delta t/T$ used are 0.8209 (for maximum $e_{rel,f}$), 0.5 (for $e_{rel,f} = e_{rel,0}$), and 0.3134 (for minimum $e_{rel,f}$) when the ZV shaper is applied; and they are 0.8519 (for maximum $e_{rel,f}$), 0.5 (for $e_{rel,f} = e_{rel,0}$), and 0.1891 (for minimum $e_{rel,f}$) when the ZVD shaper is applied.

Figures 10 and 11 show the control input components corresponding to the trajectories shown in Figs. 8 and 9 for both ZV and ZVD.

Finally, Fig. 12 illustrates the trajectory obtained using the ZVD shaper with $\Delta t/T = 0.5$ when the case 2 initial conditions are propagated through a more realistic nonlinear dynamics, including

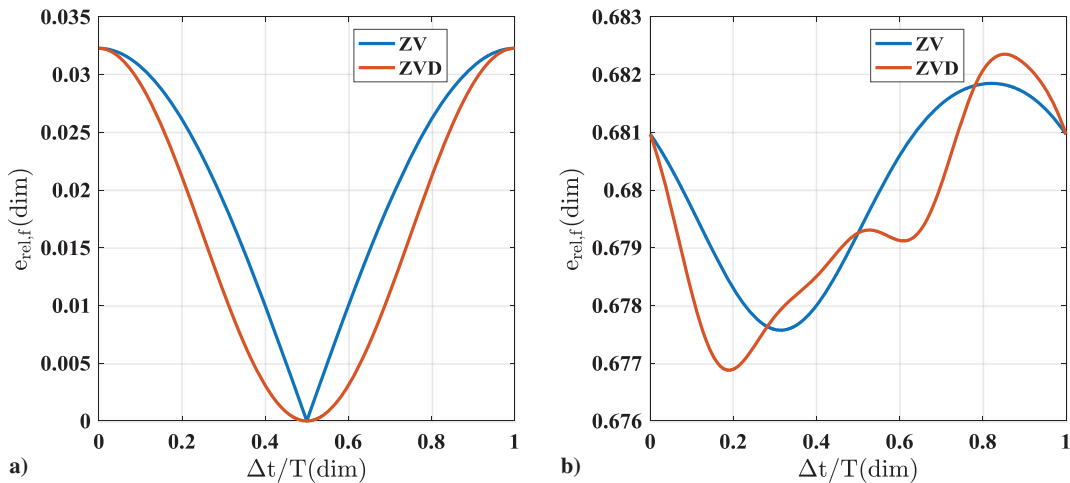


Fig. 3 $e_{rel,f}$ vs $\Delta t/T$ for a) case 1 and b) case 2.

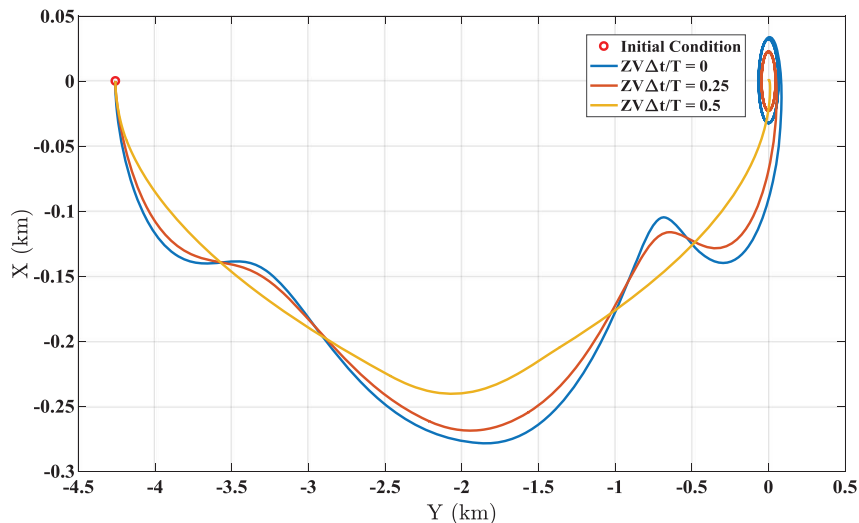


Fig. 4 Guidance trajectories given by ZV shaper for case 1, for three values of $e_{rel,f}$ ($\alpha = 45$ deg).

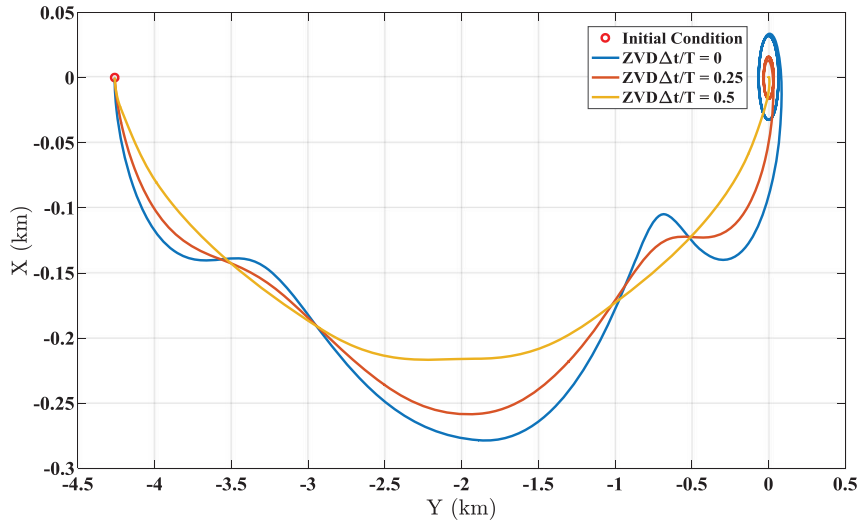


Fig. 5 Guidance trajectories given by ZVD shaper for case 1, for three values of $e_{rel,f}$ ($\alpha = 45$ deg).

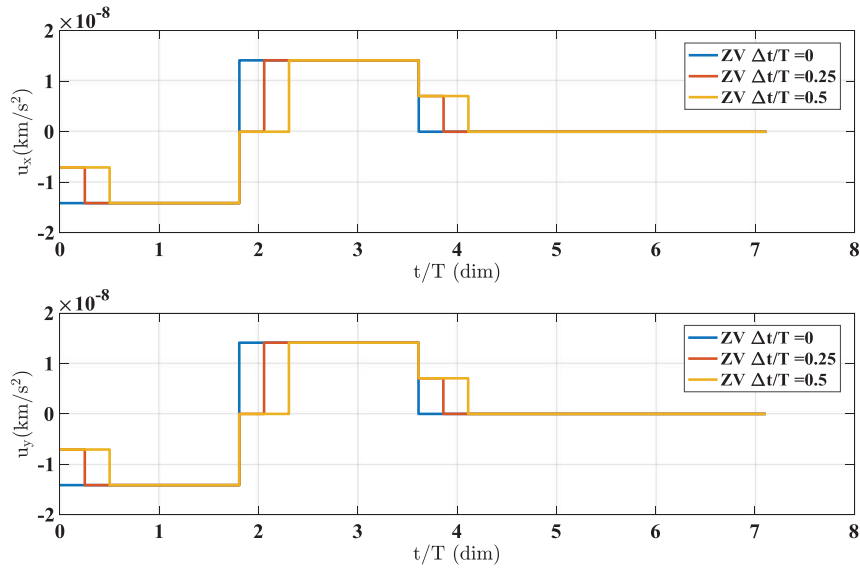


Fig. 6 Control profile shaped by ZV for case 1, for three values of $e_{rel,f}$ ($\alpha = 45$ deg).

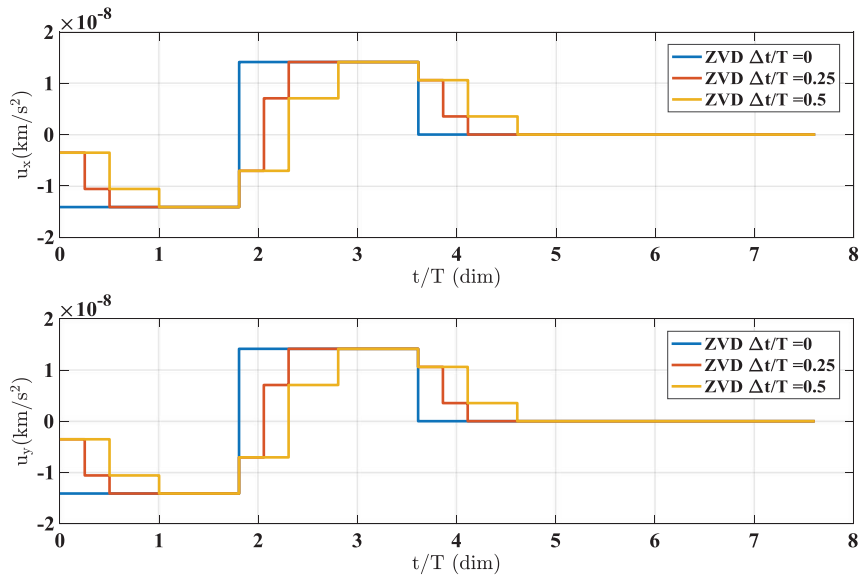


Fig. 7 Control profile shaped by ZVD for case 1, for three values of $e_{rel,f}$ ($\alpha = 45$ deg).

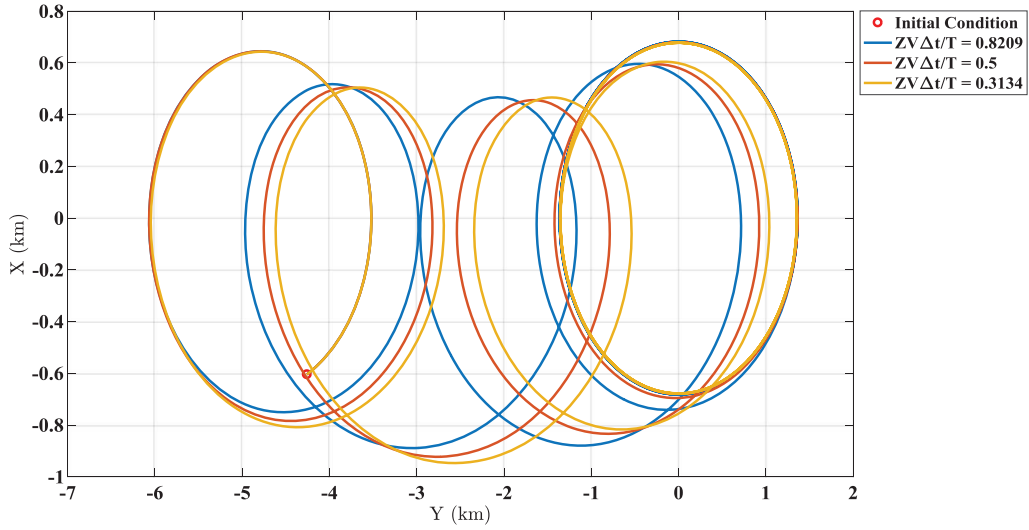


Fig. 8 Guidance trajectories given by ZV shaper for case 2, for three values of $e_{rel,f}$ ($\alpha = 45$ deg).

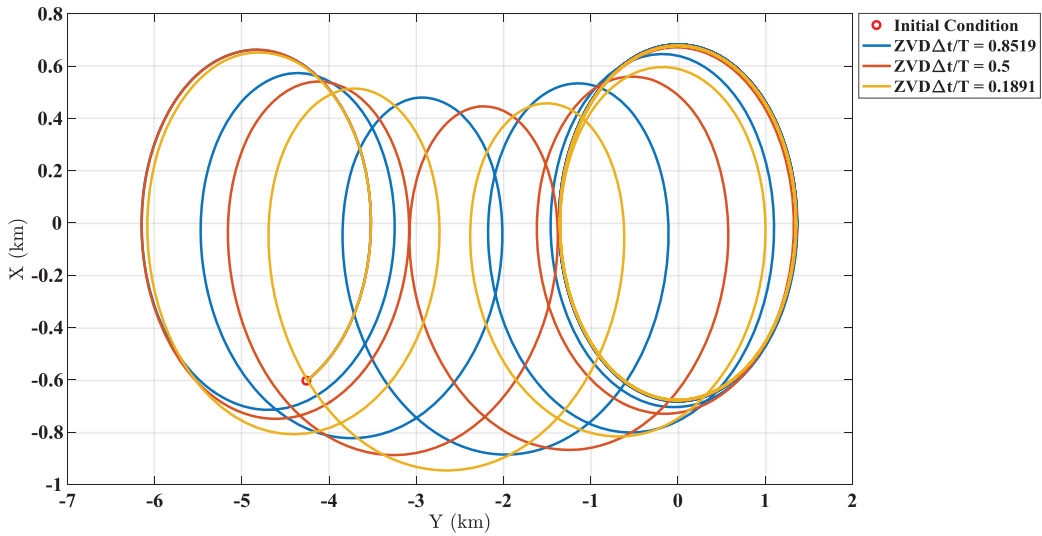


Fig. 9 Guidance trajectories given by ZVD shaper for case 2, for three values of $e_{rel,f}$ ($\alpha = 45$ deg).

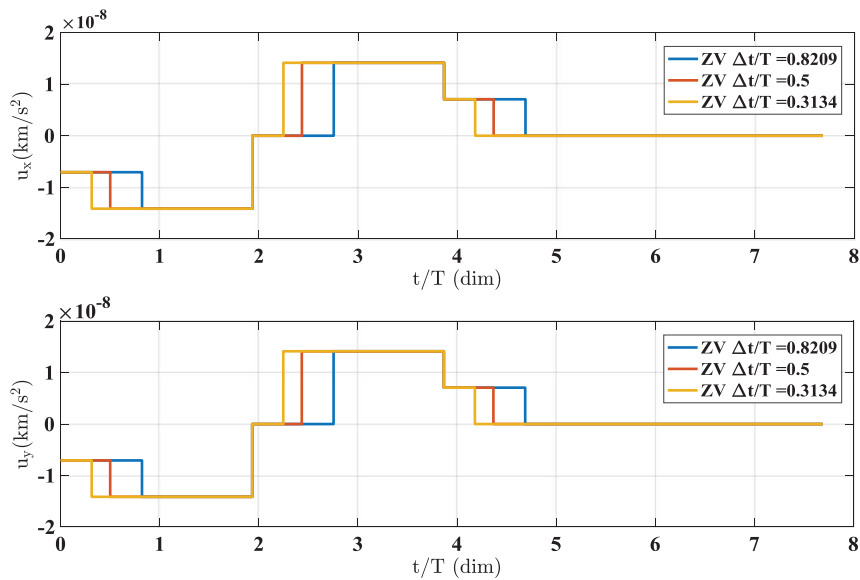


Fig. 10 Control profile shaped by ZV for case 2, for three values of $e_{rel,f}$ ($\alpha = 45$ deg).

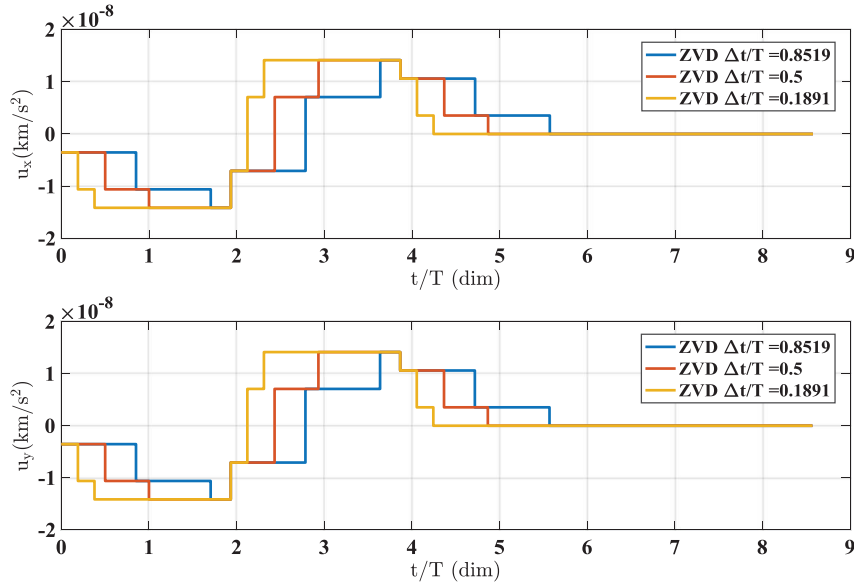


Fig. 11 Control profile shaped by ZVD for case 2, for three different values of $e_{rel,f}$ ($\alpha = 45$ deg).

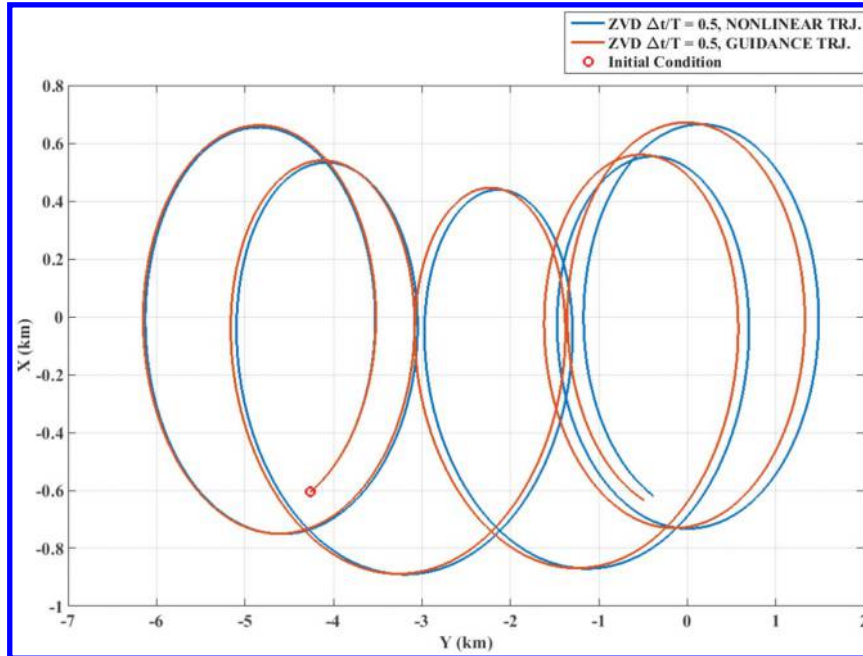


Fig. 12 Guidance and nonlinear trajectories (TRJ.) given by ZVD shaper for case 2 ($\alpha = 45$ deg).

the perturbing effects of J_2 . At the end of the maneuver (i.e., $t_m = t^* + 2\Delta t$), the position error $e_{pos} = \sqrt{x(t_m)^2 + y(t_m)^2}$ between the guidance and the nonlinear trajectory is 107 m. In addition, the center of the relative ellipse is shifted of 186 m with respect to the desired position (i.e., $\bar{y}_d = \bar{x}_d = 0$). It is worth remarking that the inclusion of J_2 through the SS dynamics model for the shaper design allows improvement of the accuracy of the guidance solution. In fact, in [8], it was shown that the guidance solution given by the ZVD shaper based on the unperturbed dynamics model provided an accuracy of 445 m.

VI. Optimized Guidance Solution

As discussed in the previous sections, the control vector U depends on shaper delay Δt and thrust angle α , once the parameters \bar{u} and \bar{y}_d are set and the initial state X_0 is given. In this study, a gradient-based algorithm is proposed to find the values of Δt and α that minimize the

maneuver cost in terms of $\Delta V = \bar{u}(t^*(\alpha) - \Delta t)$, satisfying the following constraints:

$$|e_{rel,f}(\Delta t, \alpha) - e_{rel,f,d}| = 0$$

$$\begin{cases} \frac{t^*(\alpha)}{2} - 2\Delta T > 0 & \text{for ZVD} \\ \frac{t^*(\alpha)}{2} - \Delta T > 0 & \text{for ZV} \end{cases} \quad (27)$$

where $e_{rel,f,d}$ is the desired final relative eccentricity. MATLAB's `fmincon` sequential quadratic programming routine is used to solve the preceding optimization problem. For the sake of simplicity, only the optimized solution associated with the ZVD shaper is presented hereafter. However, the same approach might be extended to the ZV-related solution.

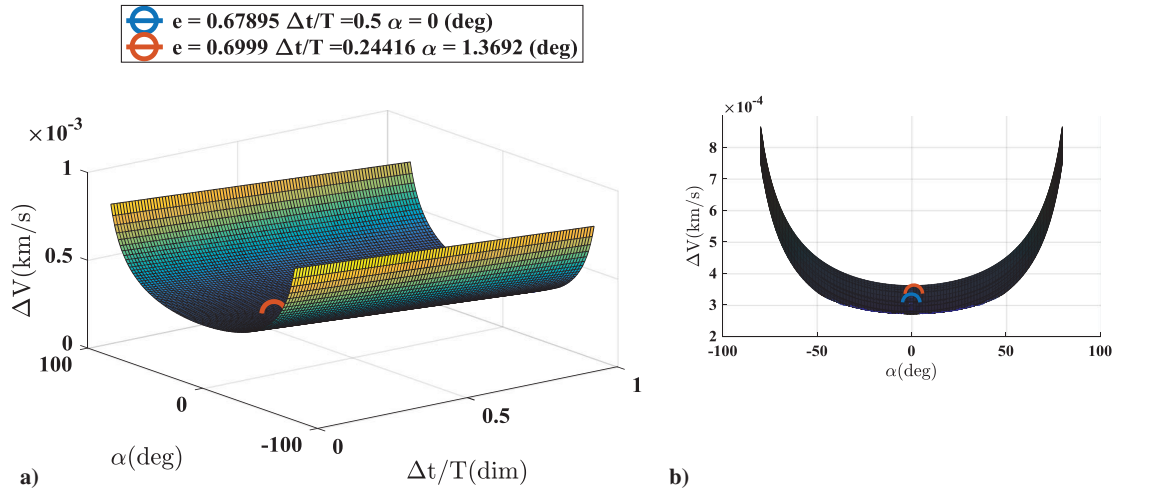


Fig. 13 Representations of a) ΔV vs α vs $\Delta t/T$; and projection of ΔV on b) ΔV - α plane, c) α - $\Delta t/T$ plane, and d) ΔV - $\Delta t/T$ plane.

To get insight into the permissible values of final relative eccentricity and facilitate the definition of space search bounds for the optimizer, a parametric analysis was carried out showing the relationships between ΔV and $e_{rel,f}$ and the optimizer variables

(α and Δt) given a set of initial conditions X_0 and the design parameters \bar{u} and \bar{y}_d . Thus, Fig. 13 shows the surface of ΔV vs α vs $\Delta t/T$, taking into account the constraints on Δt , i.e., $\Delta t < t^*/4$. For the presented analysis, the case 2 initial conditions are used. From

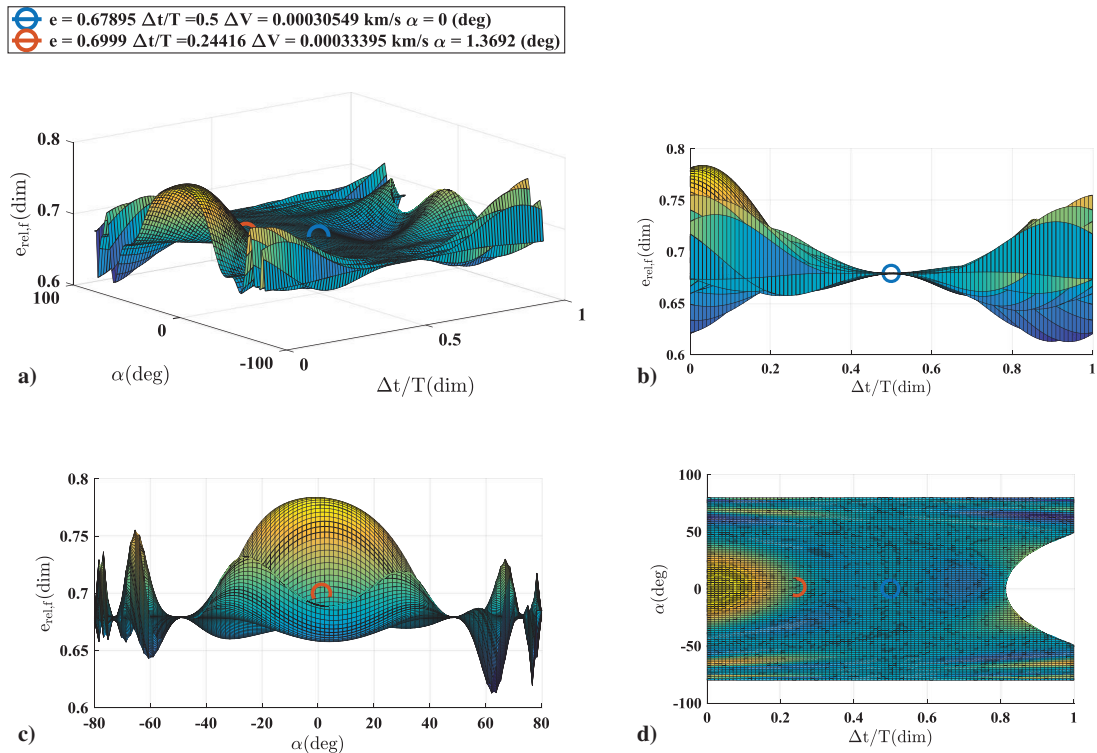


Fig. 14 Representations of a) $e_{rel,f}$ vs α vs $\Delta t/T$; and projection of $e_{rel,f}$ on b) $e_{rel,f}$ - $\Delta t/T$ plane, c) on $e_{rel,f}$ - α plane, and d) α - $\Delta t/T$ plane.

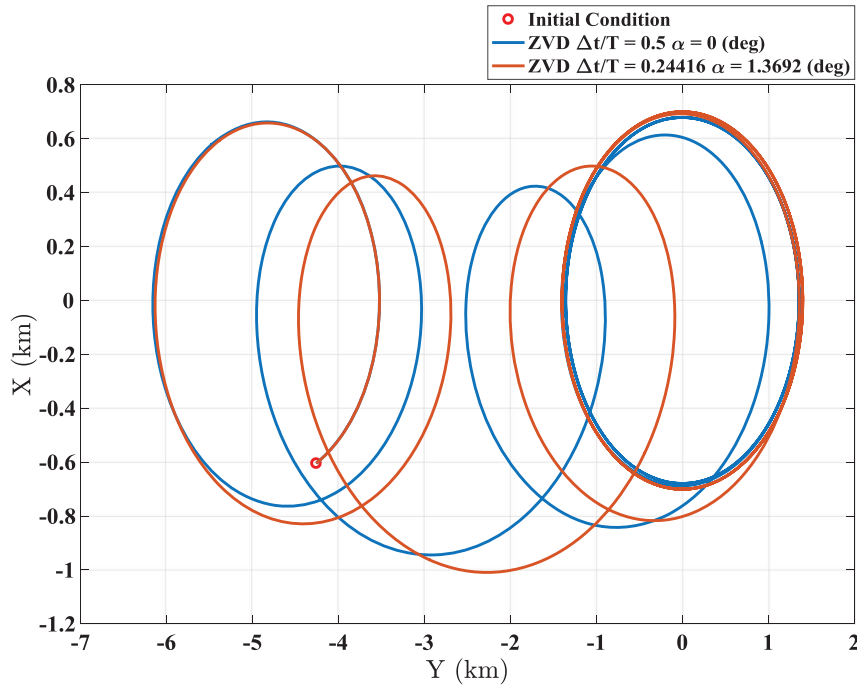


Fig. 15 Guidance trajectory.

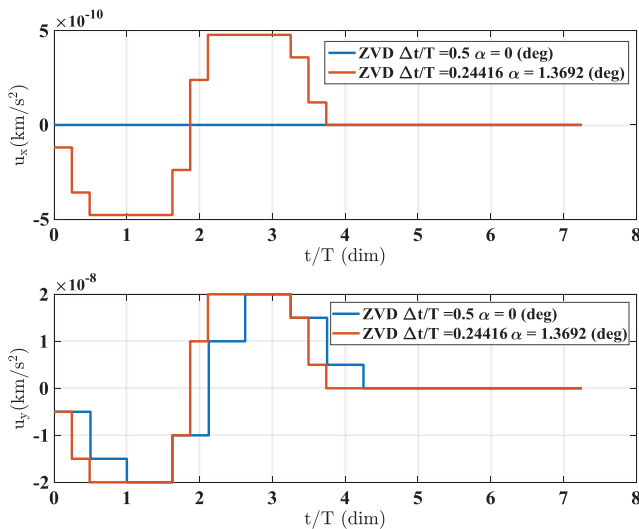


Fig. 16 Control profile.

the figure, it is straightforward that the total maneuver ΔV decreases when the thrust angle converges to zero value and the ratio $\Delta t/T$ increases up to 0.812. Figure 14 illustrates the surface of $e_{rel,f}$ vs α vs $\Delta t/T$. Again, the constraint $\Delta t < t^*/4$ is taken into account and the case 2 initial conditions are used. From the figure, it is clear that the achievable values of the final relative eccentricity by using the input-shaping based solution lie in the range $[0.6128, 0.7838]$. In addition, it is worth remarking that the parametric analysis can be exploited to determine a “good” initial guess, improving the convergence performance of the optimizer, and assess the optimizer solution.

Assuming a desired value for the final eccentricity of 0.7, the optimizer gives the solution $\Delta t/T = 0.24416$ and $\alpha = 1.3692$ deg with $\Delta V = 0.334$ m/s. This point is shown among the initial guess ($\Delta t/T = 0.5$, $\alpha = 0$ deg), which leads to $e_{rel,f} = 0.67895$ and $\Delta V = 0.305$ m/s in the plots reported in Figs. 13 and 14.

Figure 15 shows the trajectory corresponding to the initial guess ($\Delta t/T = 0.5$, $\alpha = 0$ deg) and optimized solution ($\Delta t/T = 0.24416$,

$\alpha = 1.3692$ deg). Figure 16 shows the x and y control profiles of each set of conditions over the maneuver time.

VII. Conclusions

The results presented in this Note demonstrate that input-shaping theory can be exploited to derive a general analytical guidance solution for relative orbital maneuvering as a function of shaper delay Δt and thrust angle α . The computed solutions allow a spacecraft to move from an initial location along its orbit to a desired position on the same course, as well as to fly around a desired point placed ahead or behind its initial position. It is worth remarking that the derived trajectories bring the spacecraft from an equilibrium configuration to a new equilibrium one, where equilibrium means a nondrifting relative state.

The main contribution of this Note consists of deriving an analytical guidance solution, including the effects of J_2 perturbation, for planar spacecraft rephasing and rendezvous maneuvers. This could be easily implemented on board small spacecraft with a low-thrust propulsion system and limited computing capabilities. The second important contribution is the ability to use such analytical solutions to easily and quickly compute maneuvers that require minimum fuel consumption.

Appendix A: ZV Final State

$$\begin{aligned}
 x_f = & \frac{1}{2\bar{n}^3} \left[\bar{n}\bar{u}_x + 8\bar{m}^2\bar{n}x_0 + \bar{n}\bar{u}_x \cos(\bar{n}(\Delta t + t^*)) \right. \\
 & + 2\bar{m}\bar{u}_y \sin(\bar{n}(\Delta t + t^*)) + 4\bar{m}\bar{n}\dot{y}_0 + \bar{n}\bar{u}_x \cos(\bar{n}\Delta t) \\
 & + 2\bar{m}\bar{u}_y \sin(\bar{n}\Delta t) + \bar{n}\bar{u}_x \cos(\bar{n}t^*) - 2\bar{n}\bar{u}_x \cos(\bar{n}t^*/2) \\
 & - 2\bar{n}\bar{u}_x \cos(\bar{n}(2\Delta t + t^*)/2) + 2\bar{n}^3x_0 \cos(\bar{n}(\Delta t + t^*)) \\
 & + 2\bar{m}\bar{u}_y \sin(\bar{n}t^*) - 4\bar{m}\bar{u}_y \sin(\bar{n}t^*/2) \\
 & - 4\bar{m}\bar{u}_y \sin(\bar{n}(2\Delta t + t^*)/2) + 2\bar{n}^2\dot{x}_0 \sin(\bar{n}(\Delta t + t^*)) \\
 & \left. - 8\bar{m}^2\bar{n}x_0 \cos(\bar{n}(\Delta t + t^*)) - 4\bar{m}\bar{n}\dot{y}_0 \cos(\bar{n}(\Delta t + t^*)) \right]
 \end{aligned}$$

$$y_f = \frac{1}{4\bar{n}^4} \left[8\bar{m}^2 \bar{u}_y + 4\bar{n}^4 y_0 - 8\bar{m}\bar{n}^2 \dot{x}_0 + 8\bar{m}^2 \bar{u}_y \cos(\bar{n}\Delta t) + 4\bar{n}^4 t^* \dot{y}_0 + 8\bar{m}^2 \bar{u}_y \cos(\bar{n}t^*) - 16\bar{m}^2 \bar{u}_y \cos(\bar{n}t^*/2) - 16\bar{m}^2 \bar{u}_y \cos(\bar{n}(2\Delta t + t^*)/2) - \bar{n}^4 t^{*2} \bar{u}_y + 4\Delta t \bar{n}^4 \dot{y}_0 + 8\bar{m}^2 \bar{u}_y \cos(\bar{n}(\Delta t + t^*)) - 4\bar{m} \bar{n} \bar{u}_x \sin(\bar{n}(\Delta t + t^*)) - 4\bar{m} \bar{n} \bar{u}_x \sin(\bar{n}\Delta t) + 4\bar{m}^2 \bar{n}^2 t^{*2} \bar{u}_y + 8\Delta t \bar{m} \bar{n}^4 x_0 + 8\bar{m}\bar{n}^2 \dot{x}_0 \cos(\bar{n}(\Delta t + t^*)) - 4\bar{m} \bar{n} \bar{u}_x \sin(\bar{n}t^*) + 8\bar{m} \bar{n} \bar{u}_x \sin(\bar{n}t^*/2) + 8\bar{m} \bar{n} \bar{u}_x \sin(\bar{n}(2\Delta t + t^*)/2) - 8\bar{m}\bar{n}^3 x_0 \sin(\bar{n}(\Delta t + t^*)) + 32\bar{m}^3 \bar{n} x_0 \sin(\bar{n}(\Delta t + t^*)) + 16\bar{m}^2 \bar{n} \dot{y}_0 \sin(\bar{n}(\Delta t + t^*)) + 8\bar{m}\bar{n}^4 t^* x_0 - 32\Delta t \bar{m}^3 \bar{n}^2 x_0 - 16\Delta t \bar{m}^2 \bar{n}^2 \dot{y}_0 - 32\bar{m}^3 \bar{n}^2 t^* x_0 - 16\bar{m}^2 \bar{n}^2 t^* \dot{y}_0 \right]$$

$$\dot{x}_f = \frac{1}{\bar{n}^2} \left[\bar{m} \bar{u}_y + \bar{m} \bar{u}_y \cos(\bar{n}(\Delta t + t^*)) - \bar{n} \bar{u}_x \sin(\bar{n}(\Delta t + t^*)) / 2 + \bar{m} \bar{u}_y \cos(\bar{n}\Delta t) - \bar{n} \bar{u}_x \sin(\bar{n}\Delta t) / 2 + \bar{m} \bar{u}_y \cos(\bar{n}t^*) - 2\bar{m} \bar{u}_y \cos(\bar{n}t^*/2) - 2\bar{m} \bar{u}_y \cos(\bar{n}(2\Delta t + t^*)/2) + \bar{n}^2 \dot{x}_0 \cos(\bar{n}(\Delta t + t^*)) - \bar{n} \bar{u}_x \sin(\bar{n}t^*) / 2 + \bar{n} \bar{u}_x \sin(\bar{n}t^*/2) + \bar{n} \bar{u}_x \sin(\bar{n}(2\Delta t + t^*)/2) - \bar{n}^3 x_0 \sin(\bar{n}(\Delta t + t^*)) + 2\bar{m} \bar{n} \dot{y}_0 \sin(\bar{n}(\Delta t + t^*)) + 4\bar{m}^2 \bar{n} x_0 \sin(\bar{n}(\Delta t + t^*)) \right]$$

$$\dot{y}_f = -\frac{1}{\bar{n}^3} \left[8\bar{m}^3 \bar{n} x_0 - 2\bar{m}\bar{n}^3 x_0 - \bar{n}^3 \dot{y}_0 + 4\bar{m}^2 \bar{n} \dot{y}_0 + 2\bar{m}^2 \bar{u}_y \sin(\bar{n}\Delta t) + 2\bar{m}^2 \bar{u}_y \sin(\bar{n}t^*) - 4\bar{m}^2 \bar{u}_y \sin(\bar{n}t^*/2) - 4\bar{m}^2 \bar{u}_y \sin(\bar{n}(2\Delta t + t^*)/2) + \bar{m} \bar{n} \bar{u}_x + 2\bar{m}^2 \bar{u}_y \sin(\bar{n}(\Delta t + t^*)) + \bar{m} \bar{n} \bar{u}_x \cos(\bar{n}\Delta t) + \bar{m} \bar{n} \bar{u}_x \cos(\bar{n}t^*) - 2\bar{m} \bar{n} \bar{u}_x \cos(\bar{n}t^*/2) - 2\bar{m} \bar{n} \bar{u}_x \cos(\bar{n}(2\Delta t + t^*)/2) + 2\bar{m}\bar{n}^3 x_0 \cos(\bar{n}(\Delta t + t^*)) - 8\bar{m}^3 \bar{n} x_0 \cos(\bar{n}(\Delta t + t^*)) - 4\bar{m}^2 \bar{n} \dot{y}_0 \cos(\bar{n}(\Delta t + t^*)) + 2\bar{m}\bar{n}^2 \dot{x}_0 \sin(\bar{n}(\Delta t + t^*)) + \bar{m} \bar{n} \bar{u}_x \cos(\bar{n}(\Delta t + t^*)) \right]$$

$$\begin{aligned} \bar{u}_x &= \bar{u} \sin \alpha \\ \bar{u}_y &= \bar{u} \cos \alpha \end{aligned} \tag{A1}$$

Appendix B: ZVD Final State

$$x_f = \frac{1}{4\bar{n}^3} \left[\bar{n} \bar{u}_x + 16\bar{m}^2 \bar{n} x_0 + 4\bar{n}^3 x_0 \cos(\bar{n}(2\Delta t + t^*)) + 4\bar{n}^2 \dot{x}_0 \sin(\bar{n}(2\Delta t + t^*)) + 2\bar{n} \bar{u}_x \cos(\bar{n}(\Delta t + t^*)) + 4\bar{m} \bar{u}_y \sin(\bar{n}(\Delta t + t^*)) + 8\bar{m} \bar{n} \dot{y}_0 + 2\bar{n} \bar{u}_x \cos(\bar{n}\Delta t) + \bar{n} \bar{u}_x \cos(2\bar{n}\Delta t) + 4\bar{m} \bar{u}_y \sin(\bar{n}\Delta t) + 2\bar{m} \bar{u}_y \sin(2\bar{n}\Delta t) + \bar{n} \bar{u}_x \cos(\bar{n}t^*) - 2\bar{n} \bar{u}_x \cos(\bar{n}t^*/2) + \bar{n} \bar{u}_x \cos(\bar{n}(2\Delta t + t^*)) - 4\bar{n} \bar{u}_x \cos(\bar{n}(2\Delta t + t^*)/2) - 2\bar{n} \bar{u}_x \cos(\bar{n}(4\Delta t + t^*)/2) + 2\bar{m} \bar{u}_y \sin(\bar{n}t^*) - 4\bar{m} \bar{u}_y \sin(\bar{n}t^*/2) + 2\bar{m} \bar{u}_y \sin(\bar{n}(2\Delta t + t^*)) - 8\bar{m} \bar{u}_y \sin(\bar{n}(2\Delta t + t^*)/2) - 4\bar{m} \bar{u}_y \sin(\bar{n}(4\Delta t + t^*)/2) - 8\bar{m} \bar{n} \dot{y}_0 \cos(\bar{n}(2\Delta t + t^*)) - 16\bar{m}^2 \bar{n} x_0 \cos(\bar{n}(2\Delta t + t^*)) \right]$$

$$y_f = \frac{1}{4\bar{n}^4} \left[4\bar{m}^2 \bar{u}_y + 4\bar{n}^4 y_0 - 8\bar{m}\bar{n}^2 \dot{x}_0 + 8\bar{m}^2 \bar{u}_y \cos(\bar{n}\Delta t) + 4\bar{m}^2 \bar{u}_y \cos(2\bar{n}\Delta t) + 4\bar{n}^4 t^* \dot{y}_0 + 4\bar{m}^2 \bar{u}_y \cos(\bar{n}\Delta t) - 8\bar{m}^2 \bar{u}_y \cos(\bar{n}t^*/2) + 4\bar{m}^2 \bar{u}_y \cos(\bar{n}(2\Delta t + t^*)) - 16\bar{m}^2 \bar{u}_y \cos(\bar{n}(2\Delta t + t^*)/2) - 8\bar{m}^2 \bar{u}_y \cos(\bar{n}(4\Delta t + t^*)/2) - \bar{n}^4 t^{*2} \bar{u}_y + 8\Delta t \bar{n}^4 \dot{y}_0 + 8\bar{m}^2 \bar{u}_y \cos(\bar{n}(\Delta t + t^*)) - 4\bar{m} \bar{n} \bar{u}_x \sin(\bar{n}(\Delta t + t^*)) - 4\bar{m} \bar{n} \bar{u}_x \sin(\bar{n}\Delta t) - 2\bar{m} \bar{n} \bar{u}_x \sin(2\bar{n}\Delta t) + 4\bar{m}^2 \bar{n}^2 t^{*2} \bar{u}_y + 16\Delta t \bar{m} \bar{n}^4 x_0 - 2\bar{m} \bar{n} \bar{u}_x \sin(\bar{n}t^*) + 4\bar{m} \bar{n} \bar{u}_x \sin(\bar{n}t^*/2) - 2\bar{m} \bar{n} \bar{u}_x \sin(\bar{n}(2\Delta t + t^*)) + 8\bar{m} \bar{n} \bar{u}_x \sin(\bar{n}(2\Delta t + t^*)/2) + 4\bar{m} \bar{n} \bar{u}_x \sin(\bar{n}(4\Delta t + t^*)/2) + 8\bar{m}\bar{n}^4 t^* x_0 - 64\Delta t \bar{m}^3 \bar{n}^2 x_0 - 32\Delta t \bar{m}^2 \bar{n}^2 \dot{y}_0 + 8\bar{m}\bar{n}^2 \dot{x}_0 \cos(\bar{n}(2\Delta t + t^*)) - 8\bar{m}\bar{n}^3 x_0 \sin(\bar{n}(2\Delta t + t^*)) + 32\bar{m}^3 \bar{n} x_0 \sin(\bar{n}(2\Delta t + t^*)) + 16\bar{m}^2 \bar{n} \dot{y}_0 \sin(\bar{n}(2\Delta t + t^*)) - 32\bar{m}^3 \bar{n}^2 t^* x_0 - 16\bar{m}^2 \bar{n}^2 t^* \dot{y}_0 \right]$$

$$\dot{x}_f = \frac{1}{4\bar{n}^2} \left[2\bar{m} \bar{u}_y + 4\bar{n}^2 \dot{x}_0 \cos(\bar{n}(2\Delta t + t^*)) - 4\bar{n}^3 x_0 \sin(\bar{n}(2\Delta t + t^*)) + 4\bar{m} \bar{u}_y \cos(\bar{n}(\Delta t + t^*)) - 2\bar{n} \bar{u}_x \sin(\bar{n}(\Delta t + t^*)) + 4\bar{m} \bar{u}_y \cos(\bar{n}\Delta t) + 2\bar{m} \bar{u}_y \cos(2\bar{n}\Delta t) - 2\bar{n} \bar{u}_x \sin(\bar{n}\Delta t) - \bar{n} \bar{u}_x \sin(2\bar{n}\Delta t) + 2\bar{m} \bar{u}_y \cos(\bar{n}t^*) - 4\bar{m} \bar{u}_y \cos(\bar{n}t^*/2) + 2\bar{m} \bar{u}_y \cos(\bar{n}(2\Delta t + t^*)) - 8\bar{m} \bar{u}_y \cos(\bar{n}(2\Delta t + t^*)/2) - 4\bar{m} \bar{u}_y \cos(\bar{n}(4\Delta t + t^*)/2) - \bar{n} \bar{u}_x \sin(\bar{n}t^*) + 2\bar{n} \bar{u}_x \sin(\bar{n}t^*/2) - \bar{n} \bar{u}_x \sin(\bar{n}(2\Delta t + t^*)) + 4\bar{n} \bar{u}_x \sin(\bar{n}(2\Delta t + t^*)/2) + 2\bar{n} \bar{u}_x \sin(\bar{n}(4\Delta t + t^*)/2) + 8\bar{m} \bar{n} \dot{y}_0 \sin(\bar{n}(2\Delta t + t^*)) + 16\bar{m}^2 \bar{n} x_0 \sin(\bar{n}(2\Delta t + t^*)) \right]$$

$$\dot{y}_f = -\frac{1}{2\bar{n}^3} \left[16\bar{m}^3 \bar{n} x_0 - 4\bar{m}\bar{n}^3 x_0 - 2\bar{n}^3 \dot{y}_0 + 8\bar{m}^2 \bar{n} \dot{y}_0 + 4\bar{m}^2 \bar{u}_y \sin(\bar{n}\Delta t) + 2\bar{m}^2 \bar{u}_y \sin(2\bar{n}\Delta t) + 2\bar{m}^2 \bar{u}_y \sin(\bar{n}t^*) - 4\bar{m}^2 \bar{u}_y \sin(\bar{n}t^*/2) + 2\bar{m}^2 \bar{u}_y \sin(\bar{n}(2\Delta t + t^*)) - 8\bar{m}^2 \bar{u}_y \sin(\bar{n}(2\Delta t + t^*)/2) - 4\bar{m}^2 \bar{u}_y \sin(\bar{n}(4\Delta t + t^*)/2) + \bar{m} \bar{n} \bar{u}_x + 4\bar{m}^2 \bar{u}_y \sin(\bar{n}(\Delta t + t^*)) + 2\bar{m} \bar{n} \bar{u}_x \cos(\bar{n}\Delta t) + \bar{m} \bar{n} \bar{u}_x \cos(2\bar{n}\Delta t) + \bar{m} \bar{n} \bar{u}_x \cos(\bar{n}t^*) - 2\bar{m} \bar{n} \bar{u}_x \cos(\bar{n}t^*/2) + \bar{m} \bar{n} \bar{u}_x \cos(\bar{n}(2\Delta t + t^*)) - 4\bar{m} \bar{n} \bar{u}_x \cos(\bar{n}(2\Delta t + t^*)/2) - 2\bar{m} \bar{n} \bar{u}_x \cos(\bar{n}(4\Delta t + t^*)/2) + 4\bar{m}\bar{n}^3 x_0 \cos(\bar{n}(2\Delta t + t^*)) - 16\bar{m}^3 \bar{n} x_0 \cos(\bar{n}(2\Delta t + t^*)) - 8\bar{m}^2 \bar{n} \dot{y}_0 \cos(\bar{n}(2\Delta t + t^*)) + 4\bar{m}\bar{n}^2 \dot{x}_0 \sin(\bar{n}(2\Delta t + t^*)) + 2\bar{m} \bar{n} \bar{u}_x \cos(\bar{n}(\Delta t + t^*)) \right]$$

$$\begin{aligned} \bar{u}_x &= \bar{u} \sin \alpha \\ \bar{u}_y &= \bar{u} \cos \alpha \end{aligned} \tag{B1}$$

Appendix C: Final Relative Eccentricity

$$e_{rel,f} = \sqrt{\frac{1}{4\bar{m}^2\bar{n}^6} \left[\begin{aligned} &8\bar{m}^3\bar{n}x_0 - 8\bar{m}\bar{n}^3x_0 - 4\bar{n}^3\dot{y}_0 + 4\bar{m}^2\bar{n}\dot{y}_0 + 2\bar{m}^2\bar{u}_y \sin(\Delta t\bar{n}) \\ &+ 2\bar{m}^2\bar{u}_y \sin(\bar{n}t^*) - 4\bar{m}^2\bar{u}_yD - 4\bar{m}^2\bar{u}_y \sin(C) + \bar{m}\bar{n}\bar{u}_x \\ &+ 2\bar{m}^2\bar{u}_yA + \bar{m}\bar{n}\bar{u}_x \cos(\Delta t\bar{n}) + \bar{m}\bar{n}\bar{u}_x \cos(\bar{n}t^*) - 2\bar{m}\bar{n}\bar{u}_xE \\ &- 2\bar{m}\bar{n}\bar{u}_x \cos(C) + 2\bar{m}\bar{n}^3x_0B - 8\bar{m}^3\bar{n}x_0B - 4\bar{m}^2\bar{n}\dot{y}_0B \\ &+ 2\bar{m}\bar{n}^2\dot{x}_0A + \bar{m}\bar{n}\bar{u}_xB \end{aligned} \right]^2 + \frac{\bar{m}^2}{\bar{n}^8} \left[\begin{aligned} &2\bar{m}\bar{u}_y + 2\bar{m}\bar{u}_yB - \bar{n}\bar{u}_xA + 2\bar{m}\bar{u}_y \cos(\Delta t\bar{n}) - \bar{n}\bar{u}_x \sin(\Delta t\bar{n}) \\ &+ 2\bar{m}\bar{u}_y \cos(\bar{n}t^*) - 4\bar{m}\bar{u}_yE - 4\bar{m}\bar{u}_y \cos(C) + 2\bar{n}^2\dot{x}_0B \\ &- \bar{n}\bar{u}_x \sin(\bar{n}t^*) + 2\bar{n}\bar{u}_xD + 2\bar{n}\bar{u}_x \sin(C) - 2\bar{n}^3x_0A \\ &+ 4\bar{m}\bar{n}\dot{y}_0A + 8\bar{m}^2\bar{n}x_0A \end{aligned} \right]^2}$$

where

$$\begin{aligned} A &= \sin(\bar{n}(\Delta t + t^*)) \\ B &= \cos(\bar{n}(\Delta t + t^*)) \\ C &= \frac{\bar{n}(2\Delta t + t^*)}{2} \\ D &= \sin\left(\frac{\bar{n}t^*}{2}\right) \\ E &= \cos\left(\frac{\bar{n}t^*}{2}\right) \\ \bar{u}_x &= \bar{u} \sin \alpha \\ \bar{u}_y &= \bar{u} \cos \alpha \end{aligned} \quad (C1)$$

where

$$\begin{aligned} A &= \bar{n}(2\Delta t + t^*) \\ B &= \frac{\bar{n}(4\Delta t + t^*)}{2} \\ C &= \sin(2\bar{n}\Delta t) \\ D &= \cos(2\bar{n}\Delta t) \\ E &= \cos(2\bar{n}\Delta t) \\ F &= \cos(\bar{n}t^*/2) \\ G &= \sin(\bar{n}(\Delta t + t^*)) \\ H &= \cos(\bar{n}(\Delta t + t^*)) \\ \bar{u}_x &= \bar{u} \sin \alpha \\ \bar{u}_y &= \bar{u} \cos \alpha \end{aligned} \quad (D1)$$

Appendix D: ZVD Final Relative Eccentricity

$$e_{rel,f} = \sqrt{\frac{1}{4\bar{n}^8} \left[\begin{aligned} &2\bar{m}^2\bar{u}_y + 4\bar{m}^2\bar{u}_y \cos(\Delta t\bar{n}) + 2\bar{m}^2\bar{u}_yD + 2\bar{m}^2\bar{u}_y \cos(\bar{n}t^*) \\ &- 4\bar{m}^2\bar{u}_yF + 2\bar{m}^2\bar{u}_y \cos(A) - 8\bar{m}^2\bar{u}_y \cos(A/2) \\ &- 4\bar{m}^2\bar{u}_y \cos(B) + 4\bar{m}^2\bar{u}_yH - 2\bar{m}\bar{n}\bar{u}_xG - 2\bar{m}\bar{n}\bar{u}_x \sin(\Delta t\bar{n}) \\ &- \bar{m}\bar{n}\bar{u}_xC - \bar{m}\bar{n}\bar{u}_x \sin(\bar{n}t^*) + 2\bar{m}\bar{n}\bar{u}_xE - \bar{m}\bar{n}\bar{u}_x \sin(A) \\ &+ 4\bar{m}\bar{n}\bar{u}_x \sin(A/2) + 2\bar{m}\bar{n}\bar{u}_x \sin(B) + 4\bar{m}\bar{n}^2\dot{x}_0 \cos(A) \\ &- 4\bar{m}\bar{n}^3x_0 \sin(A) + 16\bar{m}^3\bar{n}x_0 \sin(A) + 8\bar{m}^2\bar{n}\dot{y}_0 \sin(A) \end{aligned} \right]^2 + \frac{1}{16\bar{m}^2\bar{n}^6} \left[\begin{aligned} &16\bar{m}^3\bar{n}x_0 - 16\bar{m}\bar{n}^3x_0 - 8\bar{n}^3\dot{y}_0 + 8\bar{m}^2\bar{n}\dot{y}_0 + 4\bar{m}^2\bar{u}_y \sin(\Delta t\bar{n}) \\ &+ 2\bar{m}^2\bar{u}_yC + 2\bar{m}^2\bar{u}_y \sin(\bar{n}t^*) - 4\bar{m}^2\bar{u}_yE + 2\bar{m}^2\bar{u}_y \sin(A) \\ &- 8\bar{m}^2\bar{u}_y \sin(A/2) - 4\bar{m}^2\bar{u}_y \sin(B) + \bar{m}\bar{n}\bar{u}_x + 4\bar{m}^2\bar{u}_yG \\ &+ 2\bar{m}\bar{n}\bar{u}_x \cos(\Delta t\bar{n}) + \bar{m}\bar{n}\bar{u}_xD + \bar{m}\bar{n}\bar{u}_x \cos(\bar{n}t^*) - 2\bar{m}\bar{n}\bar{u}_xF \\ &+ \bar{m}\bar{n}\bar{u}_x \cos(A) - 4\bar{m}\bar{n}\bar{u}_x \cos(A/2) - 2\bar{m}\bar{n}\bar{u}_x \cos(B) \\ &+ 4\bar{m}\bar{n}^3x_0 \cos(A) - 16\bar{m}^3\bar{n}x_0 \cos(A) - 8\bar{m}^2\bar{n}\dot{y}_0 \cos(A) \\ &+ 4\bar{m}\bar{n}^2\dot{x}_0 \sin(A) + 2\bar{m}\bar{n}\bar{u}_xH \end{aligned} \right]^2}$$

Acknowledgments

The authors thank the U.S. Air Force Research Laboratory and Stanford University for sponsoring this investigation under contract number FA9453-16-C-0029. This was presented as Paper 2017 at the 27th AAS/AIAA Space Flight Mechanics Meeting in San Antonio, Texas, 6–9 February 2017.

References

- [1] Bandyopadhyay, S., Subramanian, G., Foust, R., Morgan, D., Chung, S., and Hadaegh, F., “A Review of Impending Small Satellite Formation Flying Missions,” *53rd AIAA Aerospace Sciences Meeting*, AIAA Paper 2015-1623, 2015, pp. 1–17.
doi:10.2514/6.2015-1623
- [2] Agasid, E., et al., “Small Spacecraft Technology State of the Art,” NASA, Ames Research Center, Mission Design Division Rept. NASA/TP-2015-216648/REV1, Moffett Field, CA, 2015.
- [3] Buchen, E., “SpaceWorks’ 2014 Nano/Microsatellite Market Assessment,” *Proceedings of the 28th AIAA/USU Conference on Small Satellites*, AIAA and Utah State Univ., Paper SSC14-I-3, 2014, pp. 1–5.
- [4] Chernick, M., and D’Amico, S., “New Closed-Form Solutions for Optimal Impulsive Control for Spacecraft Relative Motion,” *2016 AIAA/AAS Astrodynamics Specialist Conference*, AIAA Paper 2016-5659, 2016, pp. 1–29.
doi:10.2514/6.2016-5659
- [5] Shaub, H., Vadali, S. R., Junkins, J. L., and Alfriend, K. T., “Spacecraft Formation Flying Control Using Mean Orbit Elements,” *Journal of the Astronautical Sciences*, Vol. 48, No. 1, 2000, pp. 69–87.
- [6] Singh, T., *Optimal Reference Signal for Dynamical Systems: Theory and Application*, 1st ed., CRC Press, Boca Raton, FL, 2010, pp. 19–66, Chap. 2.
- [7] Bevilacqua, R., “Analytical Guidance Solutions for Spacecraft Planar Rephasing Via Input Shaping,” *Journal of Guidance, Control, and Dynamics*, Vol. 37, No. 3, Feb. 2014, pp. 1042–1047.
doi:10.2514/1.G000008
- [8] Bevilacqua, R., and Lovell, T. A., “Analytical Guidance for Spacecraft Relative Motion Under Constant Thrust Using Relative Orbital Elements,” *Acta Astronautica*, Vol. 102, May 2014, pp. 47–61.
doi:10.1016/j.actaastro.2014.05.004
- [9] Schweighart, S., and Sedwick, R., “A Perturbative Analysis of Geopotential Disturbances for Satellite Cluster Formation Flying,” *Proceedings of the 2001 IEEE Aerospace Conference*, Vol. 2, IEEE Publ., Piscataway, NJ, 2001, pp. 1001–1019.
doi:10.1109/AERO.2001.931281
- [10] Schweighart, S. A., and Sedwick, R. J., “High-Fidelity Linearized J Model for Satellite Formation Flight,” *Journal of Guidance, Control, and Dynamics*, Vol. 25, No. 6, 2002, pp. 1073–1080.
doi:10.2514/2.4986
- [11] Arolovich, I., and Agranovich, G., “Control Improvement of Under-Damped Systems and Structures by Input Shaping,” *Proceedings of the 8th International Conference on Material Technologies and Modeling*, Vol. 3, Israeli Ministry of Science and Technology, MMT-2014-3-1, Ariel, Israel, 2014, pp. 1–10.
- [12] Singhose, W., Singer, N., and Seering, W., “Comparison of Command Shaping Methods for Reducing Residual Vibration,” *Proceedings of the 1995 European Control Conference*, European Control Association, Rome, 1995.
- [13] Leonard, C. L., Hollister, W. M., and Bergmann, E. V., “Orbital Formation Keeping with Differential Drag,” *Journal of Guidance, Control, and Dynamics*, Vol. 12, No. 1, 1989, pp. 108–113.
doi:10.2514/3.20374
- [14] Clohessy, W. H., and Wiltshire, R. S., “Terminal Guidance System for Satellite Rendezvous,” *Journal of the Aerospace Sciences*, Vol. 27, No. 9, 1960, pp. 653–658.
doi:10.2514/8.8704

This article has been cited by:

1. Giuseppe Di Mauro, Dario Spiller, Riccardo Bevilacqua, Fabio Curti. Optimal Continuous Maneuvers for Satellite Formation Reconfiguration in J₂-perturbed Orbits . [[Citation](#)] [[PDF](#)] [[PDF Plus](#)]